THE JOURNAL OF BIOLOGICAL CHEMISTRY VOL. 287, NO. 11, pp. 7845–7858, March 9, 2012

RACK1 Promotes Non-small-cell Lung Cancer Tumorigenicity through Activating Sonic Hedgehog Signaling Pathway*[S]

Received for publication, October 19, 2011, and in revised form, January 10, 2012 Published, JBC Papers in Press, January 19, 2012, DOI 10.1074/jbc.M111.315416

Shuo Shi[‡], Yue-Zhen Deng[‡], Jiang-Sha Zhao[‡], Xiao-Dan Ji[‡], Jun Shi[§], Yu-Xiong Feng[‡], Guo Li[‡], Jing-Jing Li[‡], Di Zhu[¶], H. Phillip Koeffler[‖], Yun Zhao[**], and Dong Xie[‡1]

From the [‡]Key Laboratory of Nutrition and Metabolism, Institute for Nutritional Sciences, Shanghai Institutes for Biological Sciences, Chinese Academy of Sciences and Graduate School of Chinese Academy of Sciences, Shanghai 200031, China, the [§]Second People's Hospital of Zhuhai, 519000 Zhuhai, Guangdong, China, the [¶]Dana-Farber Cancer Institute, Boston, Massachusetts A02115, the [‖]Cancer Science Institute of Singapore, National University of Singapore, 119077 Singapore, and the [**]Key Laboratory of Molecular Cell Biology, Institute of Biochemistry and Cell Biology, Shanghai Institutes for Biological Sciences, Chinese Academy of Sciences, Shanghai 200031, China

Background: Non-small-cell lung cancer (NSCLC) is a highly lethal disease and an improved understanding of the molecular pathogenesis mechanisms is needed.
Results: RACK1 promotes NSCLC via interacting with and activating Smoothened to mediate Gli1-dependent transcription in NSCLC cells.
Conclusion: Silencing RACK1 inhibits NSCLC tumorigenicity by blocking Sonic hedgehog signaling pathway.
Significance: Highlighting RACK1 serves as a potential biomarker and a therapeutic target of NSCLC.

Non-small-cell lung cancer (NSCLC) is a deadly disease due to lack of effective diagnosis biomarker and therapeutic target. Much effort has been made in defining gene defects in NSCLC, but its full molecular pathogenesis remains unexplored. Here, we found RACK1 (receptor of activated kinase 1) was elevated in most NSCLC, and its expression level correlated with key pathological characteristics including tumor differentiation, stage, and metastasis. In addition, RACK1 activated sonic hedgehog signaling pathway by interacting with and activating Smoothened to mediate Gli1-dependent transcription in NSCLC cells. And silencing RACK1 dramatically inhibited *in vivo* tumor growth and metastasis by blocking the sonic hedgehog signaling pathway. These results suggest that RACK1 represents a new promising diagnosis biomarker and therapeutic target for NSCLC.

Non-small-cell lung cancer (NSCLC)[2] is the leading cause of cancer deaths worldwide, with less than 15% of patients surviving beyond 5 years. Cytotoxic chemotherapy remains the therapeutic foundation of treatment in both the adjuvant and metastatic settings (1–4). These therapies are toxic and almost never curative of metastatic disease. Therefore, novel molecular targets are needed to formulate new approaches to this devastating disease.

The adaptor protein RACK1 (Receptor of Activated Kinase 1) was originally identified as a 36-kDa intracellular receptor for protein kinase C (PKC). It interacts with several protein kinases C family members (*e.g.* PKCα, PKCβII, PKCϵ, PKCδ) to regulate several signal pathways (5–11). RACK1 is a member of the WD40 superfamily of proteins with a propeller-like structure of seven WD40 repeats, including the β subunit of G-proteins (12). To our knowledge, RACK1 is ubiquitously expressed and has been implicated in a variety of cellular processes including regulation of protein translation (13–15), cellular stress (1), tissue development (2–5), and mammalian circadian clock (6, 7) as well as cancer progression (22–28).

The Hedgehog (Hh) signaling pathway controls cell proliferation (8) and differentiation during embryonic development (9–11), and it contributes to tumorigenesis when it is either mutated or misregulated (12–14). Recent evidence suggests that Hedgehog signaling may contribute to NSCLC (15, 16). When Hh ligands bind and inactivate the Hh receptor Patched-1 (PTC1), PTC1 loses its catalytic inhibition of the G-protein-coupled receptor-like signal transducer Smoothened (Smo), which triggers the transcriptional activation of the Hh target gene, a zinc finger transcription factor glioma-associated oncogene-1 (Gli1). Therefore, measurement of Gli1 mRNA levels is a reliable indicator of activity of this pathway (17).

We found that RACK1 was up-regulated in NSCLC samples, and its expression correlated with the key clinical parameters: tumor stage, metastasis, and degree of differentiation. Silencing of RACK1 promoted cancer cell apoptosis and inhibited cell proliferation and migration *in vitro* as well as abolished tumor

* This work was supported by National Basic Research Program of China Grant 2010CB912102, Ministry of Science and Technology Key Program 2012ZX10002009-017, National Natural Science Foundation of China 30930023, 90813023, Y239X31111, 81021002, 31100551, 81021002, and 81070325, National Natural Science Funds for Distinguished Young Scholar Grant 30725010, and Nature Science Foundation of China-Guangdong Joint Fund U0932001.
[S] This article contains supplemental Table 1 and Figs. 1–5.
[1] To whom correspondence should be addressed: Laboratory of Molecular Oncology, Institute for Nutritional Sciences, Shanghai Institutes for Biological Sciences, Chinese Academy of Sciences, 294 Tai-Yuan Rd., Shanghai 200031, People's Republic of China. Tel.: 86-21-54920918; Fax: 86-21-54920291; E-mail: dxie@sibs.ac.cn.
[2] The abbreviations used are: NSCLC, non-small-cell lung cancer; RACK1, receptor of activated kinase 1; SMO, Smoothened; PTC, Patched; Gli1, Glioma-associated oncogene-1; Hh, Hedgehog; SHH, sonic hedgehog; IB, immunoblot; MTT, 3-(4, 5-dimethylthiazol-2-yl)-2,5-diphenyltetrazolium bromide.

growth and metastasis *in vivo*. Furthermore, we found that RACK1 expression correlated with elevated Gli1 levels in NSCLC, and Gli1 function was required for RACK1 oncogenic effects. RACK1 was found to activate Gli1 transcription via interacting and activating Smoothened, a key positive regulator in the Sonic Hedgehog signaling pathway. Taken together, our study strongly demonstrated that RACK1 is both a potential biomarker and a therapeutic drug target for NSCLC.

EXPERIMENTAL PROCEDURES

Constructs—Polymerase chain reaction (PCR) fragment corresponding to the cDNA coding for either full-length or for different regions of RACK1 were inserted into the PCMV-Myc expression vector (Clontech). The cDNA fragments coding for the full-length, the C-tail, or fragment without the C-tail of Smoothened were amplified by PCR and introduced into the PCMV-Tag4B expression vector (Stratagene). RACK1 full-length cDNA fragments were amplified by PCR and introduced into the pGEX-4-T1 vector (Amersham Biosciences) to produce GST-RACK1 fusion proteins in the BL20 *Escherichia coli* strain. Luciferase full-length cDNA was cloned into FG12 expressing construct (kindly provided by Dr. Le) and used for lentivirus package. Both A549 RACK1 siRNA control and RACK1 siRNA-containing cells were infected by FG12-luciferase lentivirus for metastasis assay. PCMV-FLAG-Gli1 was subcloned from SRαGLI1-expressing construct (kindly provided by Dr. Ariel Ruiz i Altaba) and introduced into the PCMV-Tag2B vector (Stratagene).

Cell Lines and Human Samples—The human non-small-cell lung cancer cell lines H520 and H23 were purchased from Cell Bank of Type Culture Collection of Chinese Academy of Sciences, Shanghai Institute of Cell Biology, Chinese Academy of Sciences. A549 cell line was a gift from Dr. Hongbing Ji. These cells were cultured in RPMI 1640 medium (Invitrogen) supplemented with 10% fetal bovine serum (Biochrom AG) at 37 °C in a humidified atmosphere containing 5% CO_2. Fresh-frozen primary NSCLCs tissues and their paired normal samples were obtained from patients undergoing surgical resection at Shanghai Chest Hospital (Shanghai, China) after consent was obtained from the patients. None of the patients received any prior radiochemotherapy.

Reagents—Murine anti-Myc and anti-FLAG monoclonal antibodies and rabbit anti-Smoothened polyclonal antibody were purchased from Santa Cruz Biotechnology (Western blot and immunoprecipitation). Rabbit anti-Gli1 polyclonal antibody for Western blot was from Cell Signaling. Rabbit anti-Gli1 and anti-Smoothened polyclonal antibodies for immunofluorescence and immunohistochemical staining were obtained from Abcam. Murine anti-RACK1 and anti-cleaved polyadenosine diphosphate-ribose polymerase and anti-E-cadherin and N-cadherin antibodies were from BD Biosciences. The dual luciferase system was purchased from Promega. Lipofectamine 2000 and TRIzol reagent were from Invitrogen. Luciferin was purchased from Xenogen Biotechnology.

RT- and Quantitative Real-time RT-PCR—Total RNA was isolated from NSCLC cell lines and tissues of NSCLC patients according to the methods described by Wang *et al.* (47). Human primer sequences were 5′ to 3′: RACK1 forward (TCTCTTTCCAGCGTGGCCATTAGA) and RACK1 reverse (CCTCGAAGCTGTAGAGATTCCGACAT); Gli1 forward (GGGATGATCCCACATCCTCAGTC and Gli1 reverse (CTGGAGCAGCCCCCCCAGT); PTCH1 forward (CCACAGAAGCGCTCCTACA) and PTCH1 reverse (CTGTAATTTCGCCCCTTCC); FOXM1 forward (GCGACTCTCGAGCATGGAGAATTGTCACCTG) and FOXM1 reverse (GCGCTACTCGAGTTCGGTTTTGATGGT); BMI1 forward (TTCATTGATGCCACAACA) and BMI1 reverse (CCATTGGCAGCATCAGC); β-actin forward (GATCATTGCTCCTCCTGAGC) and β-actin reverse (ACTCCTGCTTGCTGATCCAC). Amplification reactions were performed in a 15-μl volume of a mixture with 10 pM primer, 2 mM $MgCl_2$, 200 μM dNTP mixtures, 0.5 units of TaqDNA polymerase, and 1× buffer. All of the reactions were performed in triplicate in Mx3000 system (Stratagene). The relative mRNA level of target genes to that of β-actin in clinical samples was calculated according to the methods described by Qiu *et al.* (1). The statistical results were considered significant at $p < 0.05$ and highly significant at $p < 0.01$. All data analyses were done using the program SPSS.

Immunoprecipitations—NSCLC cells were washed with ice-cold PBS and harvested in 500 μl of IP lysis buffer (150 mM NaCl, 50 mM Tris-HCl, pH 7.5, 0.1% Nonidet P-40,1 mM EDTA, 10% glycerol supplemented with protease inhibitors). 200 ng ~ 1 μg-specific antibodies were added to cell lysates. After incubation at 4 °C overnight, 60 μl of 50% protein A or protein G-agarose was added followed by 4 h of incubation at 4 °C. Samples were centrifuged and washed 5 times with 1 ml of lysis buffer. Immunoprecipitated proteins were eluted by the addition of 40 μl of SDS sample buffer. Initial lysates and immunoprecipitated proteins were analyzed by SDS-PAGE and immunoblotted using specific antibodies.

GST Pulldown Assays—The RACK1 full-length cDNA fragment was amplified by PCR and introduced into the pGEX-4-T1 vector (Amersham Biosciences) to produce GST-RACK1 fusion proteins in the BL20 *E. coli* strain with 0.1 mM isopropyl 1-thio-β-D-galactopyranoside (Amresco) inducement. The fusion protein was purified using glutathione-Sepharose 4B (GE Healthcare), as indicated by the manufacturer. Purified recombinant proteins were analyzed by SDS-PAGE followed by Coomassie Brilliant Blue staining. A549 cells were washed with ice-cold PBS and harvested in 500 μl of GST pulldown lysis buffer (50 mM Tris-Cl, pH 7.5, 150 mM NaCl, 0.1% Nonidet P-40 and protease inhibitor mixture). 5 μg of GST-RACK1 fusion protein and cell lysates were incubated at 4 °C overnight. 20 μl of glutathione-Sepharose-4B beads were added to the samples and incubated at 4 °C for 3 h to capture the GST fusion proteins. After washing with lysis buffer five times, the proteins were eluted in Laemmli buffer and analyzed by SDS-PAGE followed by immunoblot (IB) assay.

RNA Interference of RACK1—Two target sequences for RACK1 small interfering RNA were: RACK1-RNAi-6# (the underlined sequence was the complementary sequence with RACK1 mRNA; 5′-ACCGACCATCATCATGTGGAAATTCAAGAGATTTCCACATGATGATGGTTTTTTTGGATCCC-3′ and (5′-TCGAGGGATCCAAAAAGACCACATCATGTGGAAATCTCTTGAATTTCCACATGATGATGGT-3′) and RACK1-RNAi-31# (the underlined sequence was the

complementary sequence with RACK1 mRNA; 5′-ACCGGCAAACACCTTTACACGCTTCAAGAGAGCGTGTAAAGGTGTTTGCTTTTTTGGATCCC-3′ and 5′-CGAGGGATCCAAAAAGGCAAACACCTTTACACGCTCTCTTGAAGCGTGTAAAGGTGTTTGC-3′); RACK1-RNAi-Con (the underlined sequence was the random sequence as control that was not related to RACK1 mRNA; 5′-ACCGGTACATAGGGACGTAACGTTCAAGAGACGTTACGTCCCTATGTACCTTTTTGGATCCC-′ and 5′-TCGAGGGATCCAAAAAGGTACATAGGGACGTAACGTCTCTTGAACGTTACGTCCCTATGTAC-3′). FG12 RNAi vector was used to produce small double-stranded RNA (small interfering RNA) to inhibit target gene expression in NSCLC cells.

Luciferase Reporter Assay—NSCLC cells were plated at a subconfluent density, and HH reporter assays were performed using 0.1 μg of GLIBS-Luc reporter construct or TK-luciferase control plasmid (gift from Dr. D. J. Robbins), 0.5 μg of expression vector, and 0.02 μg of Renilla luciferase pRL-TK (internal control for transfection efficiency). Cell lysates were prepared 24 h after transfection, and the reporter activity was measured using the dual -luciferase reporter assay system (Promega).

Western Blot—Cultured cells were washed twice with PBS and lysed in radioimmune precipitation assay buffer for 30 min on ice. Cell lysates were clarified by centrifugation (10,000 $\times$ *g*, 15 min), and protein concentrations were determined using the Bradford reagent (Sigma). Lysates were separated on 8 or 15% SDS-PAG; proteins were transferred to Immobilon membrane (Millipore, Bedford, MA) immunoblotted with specific primary antibodies and incubated with corresponding horseradish peroxidase-conjugated secondary antibody. All immunoblots were visualized by enhanced chemiluminescence (Pierce).

Sonic Hedgehog (SHH) and Cyclopamine Treatments—Commercial N-SHH (R&D Systems) was used at 50 nM. Cyclopamine (Sigma) was used at 8 μM. Treated cells were in 2.5% serum for 48 h instead of the usual 10% routinely used for standard growth.

Immunofluorescence—Forty-eight hours after plating on cover slides, these cells were washed 3 times with ice-cold PBS and fixed either in cold methanol at −20 °C for 5 min or in 4% formaldehyde for 20 min. Cells were permeabilized with PBS, 0.1% Triton X-100 for 1 min, and nonspecific binding sites were blocked with 3% BSA in PBST (PBS with 0.5% Tween 20). Cells were stained with primary antibodies diluted in 3% BSA, PBST overnight at 4 °C. After washing 4 times in PBST, cells were incubated for 1 h with the secondary antibody (Alexa Fluor 488-conjugated donkey anti-mouse IgG (Molecular Probes) or Alexa Fluor 555-conjugated goat anti-rabbit IgG (Molecular Probes)) in 3% BSA, PBST at a 1:1000 dilution. Fluorescence was monitored by an inverted confocal laser microscopy (Carl Zeiss, New York, NY).

3-(4,5-Dimethylthiazol-2-yl)-2,5-diphenyltetrazolium Bromide (MTT) Assay—Cells were plated in 96-well plates with a concentration of 1000 cells per well. To measure cell growth, 20 μl of 5 mg/ml MTT was added into the media and cultured at 37 °C. After 4 h, the media were removed, 200 μl of DMSO was added to dissolve the generated deposits, and the absorbance at 550 nm was measured by an automatic microplate reader. The measurement process was performed every 24 h for 5 or 7 days to generate a cell growth curve.

Apoptosis Analysis—NSCLC cells were plated in 60-mm dishes and trypsinized when they reached 70% confluence. Quantitation of apoptotic cells under hypoxic and normoxic conditions was obtained using the annexin V-PE detection kit (Beyotime) according to the manufacturer's protocol.

Cell Migration Assay—The migration assay was carried out using a 12-well Boyden Chamber (Neuro Probe) with an 8-μm pore size. Approximately 1×10^5 cells were seeded into upper wells of the Boyden Chamber and incubated for 6 h at 37 °C in medium containing 1% FBS. Medium with 10% FBS was used as a chemoattractant in the bottom wells. Cells that did not migrate through the pores of the Boyden Chamber were manually removed with a rubber swab. Cells that migrated to the lower side of the membrane were stained with hematoxylin and eosin and photographed using an inverted microscope.

In Vivo Tumorigenicity Assay—Five-week-old male nude mice were housed under standard conditions. A549 and H23 cells were trypsinized and washed with PBS and suspended in RPMI 1640 without serum. 5×10^6 of these cells were injected into the flanks of nude mice. Tumor growth was measured every 7 days, and tumor volume was estimated as length $\times$ width $\times$ height $\times$ 0.5236. Tumors were harvested from ether-anesthetized mice. All procedures were in agreement with SIBS Guide for the Care and use of Laboratory Animals and approved by the Animal Care and use Committee, Shanghai Institutes for Biological Sciences.

In Vivo Metastasis Assay—The A549 cell line was labeled with luciferase-expressing lentivirus containing an independent open reading frame of GFP. Luciferase expression was determined by using luciferin (Xenogen, Alameda, CA) and an *in vivo* imaging system (Xenogen). The luciferase-expressing A549 of RACK1-RNAi-Con and RACK1-RNAi-6# (1×10^6 in 200 μl PBS) were injected into the left ventricle of the nude mice. The metastatic lesions were monitored weekly. An aqueous solution of luciferin (150 mg/kg intraperitoneally) was injected 10 min before imaging, and then the mice were anesthetized with Forane (Abbott). The mice were placed into a light-tight chamber of the CCD camera system (Xenogen), and the photons emitted from the luciferase-expressing cells within the animal were quantified for 1 min using the software program Living Image (Xenogen) as an overlay on Igor (Wavemetrics, Seattle, WA).

Statistical Analysis—Statistical analyses were performed using Student's *t* test or analysis of variance. Data were represented as the mean $\pm$ S.E. from at least three independent experiments and considered significant when p values were < 0.05(*) or < 0.01(**).

RESULTS

RACK1 Is Up-regulated in NSCLC and Correlates with Clinical Features of NSCLC Patients—To identify the potential roles of RACK1 in the development and progression of NSCLC, we assessed its expression level by real-time polymerase chain reaction (PCR) in 63 pairs of matched lung tissue samples. Expression levels of RACK1 were significantly higher in 48 of 63 NSCLC tumors compared with their normal lung counterparts

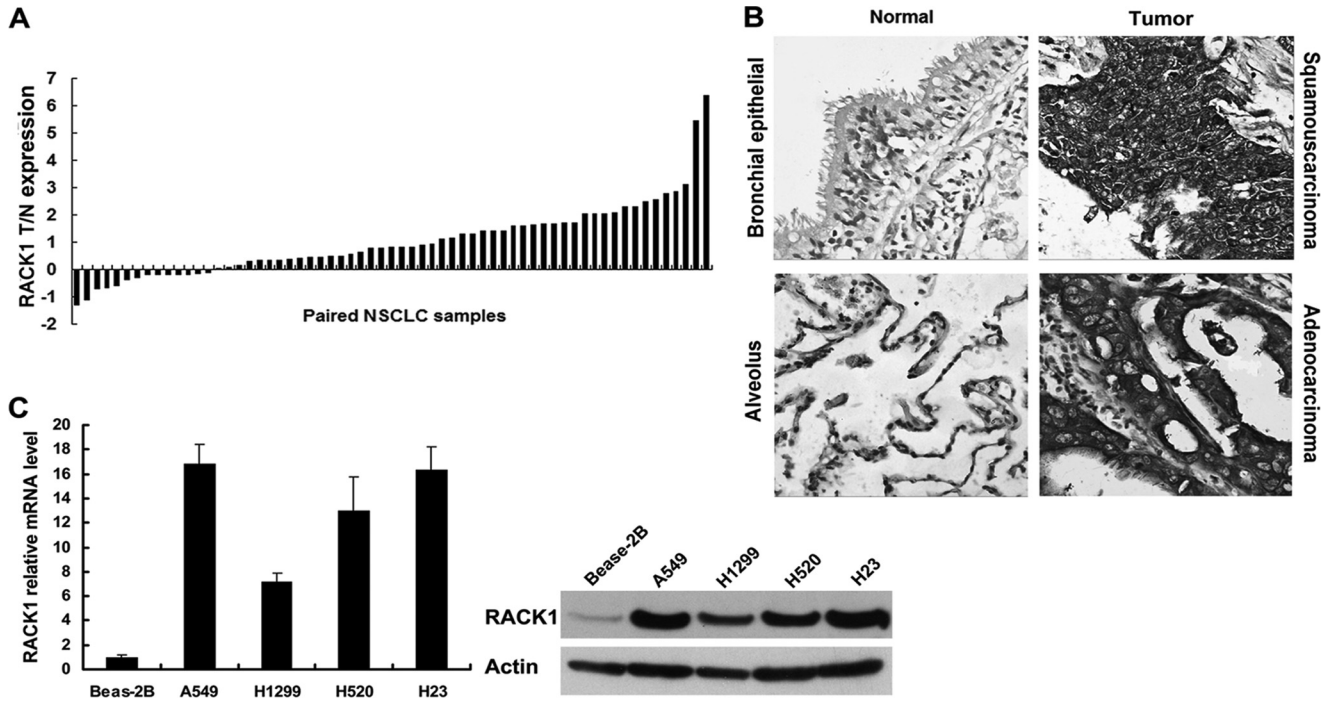

FIGURE 1. **Levels of RACK1 are increased in NSCLC clinical samples.** *A*, shown are quantitative real time PCR results of relative expression level of RACK1 in 63 pairs of NSCLC and normal lung samples. The mRNA expression level of β-actin was quantified as an internal standard and used to normalize the level of RACK1 from the same sample. Data were calculated from triplicates. Each *bar* is the $\log_2$ value of the ratio of RACK1 expression levels between NSCLC (*T*) and matched normal tissues (*N*) from the same patient. A <2-fold change in the ratio between tumor and normal tissue is <2. Because $\log_2 2 = 1$, bar value >1 represents a >2-fold increase (T > N), whereas bar value <−1 represents a >2-fold decrease (T < N). *B*, shown are immunohistochemical results of RACK1 expression in NSCLC and matched normal lung tissues. In cancer tissue from individuals with NSCLC, intense RACK1 immunoreactivity (*gray*) was observed. In corresponding paired normal tissues, however, RACK1 expression was weaker. *C*, *left bar graph* shows quantitative RT-PCR of RACK1 expression in one normal lung epithelial cell line Bease-2B and four human NSCLC cell lines (A549, H1299, H23, adenocarcinoma cell lines; H520, squamous carcinoma). The mRNA level of BEAS-2B was normalized to 1. A Western blot shows protein levels of RACK1 in BEAS-2B and human NSCLC cell lines (*right*). β-Actin was used as a loading control.

and was 2- and 4-fold higher in ~57 and 24% of the tumors compared with the normal respiratory epithelium, respectively (Fig. 1*A*). Furthermore, elevated levels of RACK1 protein were found in NSCLC tumors compared with the paired normal tissues from the same patients as shown by immunochemical staining (Fig. 1*B*). Moreover, we also examine the expression of RACK1 in NSCLC cell lines and a normal lung epithelial cell line BEASE-2B by both real time RT-PCR and Western blotting. The expression of RACK1 was dramatically elevated in the NSCLC cell lines compared with BEASE-2B control cells (Fig. 1*C*, *left* and *right panels*). Taken together, expression of RACK1 was up-regulated in both clinical samples and cell lines of NSCLC.

Further analysis revealed that the up-regulation of RACK1 mRNA in NSCLC samples was inversely correlated with differentiation of the tumors ($p = 0.000001$) and positively correlated with both tumor metastasis ($p = 0.0000348$) and tumor TNM stage ($p = 0.0000128$; Table 1). No correlations occurred between RACK1 mRNA levels and tumor type, smoking history, patient age, or gender. These data suggested that RACK1 expression correlates with advanced NSCLC.

Knockdown of Expression of RACK1 in NSCLC Cells Promotes Apoptosis and Retards Cellular Proliferation and Migration in Vitro as Well as Inhibits Tumor Growth and Metastasis in Vivo—To understand the function of RACK1 in NSCLC, we used RNAi-mediated knockdown lentiviral vector to decrease the basal level of RACK1 (knockdown of RACK1) in two non-small-cell lung cancer cell lines, A549 and H23. Western blot results showed that two independent target sequences 6# (Si RACK1 6#) and 31# (Si RACK1 31#) markedly decreased the expression of RACK1 compared with the control sequence (*Si Con*) (Fig. 2*F*). Knockdown of RACK1 significantly increased cell apoptosis (Fig. 2*A* and supplemental Fig. 1, *A* and *B*) and inhibited cell growth (Fig. 2*B*) and migration (Fig. 2*D*) *in vitro*. Furthermore, silencing of RACK1 dramatically retarded NSCLC tumor growth (Fig. 2*C*) and attenuated metastatic potential of A549 cells *in vivo* (Fig. 2*E*). Consistent with these biological phenotypes, silencing RACK1 effectively increased the level of cleaved polyadenosine diphosphate-ribose polymerase (a sensitive marker of apoptosis) as well as elevated levels of E-cadherin and lowered levels of N-cadherin (two proteins important in cell migration) (Fig. 2*F*). In summary, these data support the hypothesis that RACK1 expression is required for development and progression of NSCLC.

RACK1 Activates the Sonic Hedgehog Signaling Cascade—Data have suggested that development of the NSCLC recapitulates events important in embryonic lung development (18, 19). Additional studies have noted that the development and progression of NSCLC is associated with three crucial developmentally regulated pathways (20–22): Hedgehog (23–26), Notch (27), and Wnt (28–31) signaling pathways. Luciferase activity assays were used to identify which signal pathways were enhanced by RACK1 to foster the development of NSCLC. We transiently transfected RACK1 into three different NSCLC cell

TABLE 1

Relationship between levels of expression of RACK1 in NSCLC and clinical and pathological features

Grade of tumor differentiation, tumor type, and metastasis was determined by the pathologists. Tumor stages were classified according to the tumor node metastasis (TNM) classification of the American Joint Committee on Cancer and the International Union. Tumor size was measured by surgeons.

Clinical characteristics	No. patients	RACK1 negative ($n = 15$)	RACK1 positive ($n = 48$)	Spearman's ρ
Gender				
Male	40	10	30	$p = 0.774$
Female	23	5	18	
Age				
≤60	29	8	21	$p = 0.523$
>60	34	7	27	
Tumor type				
Squamous carcinoma	16	4	12	$p = 0.879$
Adenocarcinoma	41	9	32	
Adenosquamouscarcinoma	6	2	4	
Metastasis				
N0	30	14	16	$p = 3.48e\text{-}005$[a]
N1 and N2	26	1	25	
M1	7	0	7	
Smoke				
No	35	7	28	$p = 0.436$
Yes	28	8	20	
Tumor differentiation				
Well	10	8	2	$p = 1e\text{-}006$[a]
Moderate	14	5	9	
Poor	39	2	37	
Tumor size				
<3 cm	19	6	13	$p = 0.349$
≥3 cm	44	9	35	
TNM stage				
I	10	6	4	$p = 1.28e\text{-}005$[a]
II	20	8	12	
III	26	1	25	
IV	7	0	7	

[a] $p < 0.01$ are set for significant and highly significant difference, respectively, by Spearman's ρ test.

lines, H23, A549, and H520, and found that enforced RACK1 expression strongly activated a multimerized GLI-binding motif (GLIBS)-luciferase reporter compared with controls, but under similar experimental conditions RACK1 did not stimulate either a Notch1-luciferase reporter or a TCF-dependent Top Flash reporter (supplemental Fig. 2). Therefore, RACK1 appears to help enhance the SHH pathway in NSCLC. To help to confirm this hypothesis, we transfected increasing amounts of a RACK1 expression vector into three different NSCLC cell lines (A549, H23, and H520) and found GLIBS luciferase activity was enhanced in a RACK1 dose-dependent manner (Fig. 3*A*). Furthermore, knockdown of RACK1 strongly decreased the activity of GLI-binding site luciferase either with or without Shh-N treatment of these cell lines (Fig. 3*B*). Also, knockdown of RACK1 greatly decreased mRNA expression of the SHH target gene Gli1 as well as Gli1 target genes PTC-1, FOXM1, and BMI1 (Fig. 3*C*). In addition, knockdown of RACK1 also dramatically decreased Gli1 protein expression levels either with or without Shh-N treatment (Fig. 3, *D* and *E*). Gli1 exerts its oncogenic effects after translocating from cytoplasm to nucleus to activate GLI-mediated transcription targets including Gli1 itself. Activated Shh-N can cause Gli1 nuclear translocation. We observed that knockdown of RACK1 decreased Gli1 protein accumulation in the nucleus after Shh-N treatment, therefore, blocking Gli1 transcriptional activity (Fig. 3*F*). Together, these results strongly suggest that knockdown of RACK1 reduced Gli1 expression and inhibited the SHH signaling cascade in NSCLC cells.

Oncogenic Effects of RACK1 Are Mediated by Gli1—We next sought to explore if the oncogenic effects of RACK1 are mediated by activation of the SHH/GLI signaling pathway. Hh inappropriate activation has been linked to several types of human cancers. For example, basal cell carcinomas often have mutations in components of the Hh pathway causing the activation of Hh (32). Also, Hh ligand-dependent cancers may respond to Hh ligand in either an autocrine or paracrine manner (33, 34). Lung tumors have been proposed to respond to Hh mainly in an autocrine manner, as these tumors can produce, secrete, and respond to Hh, which may stimulate their proliferation and/or survival (17).

To address the contribution of Gli1 transcription to the oncogenic effects of RACK1, we ectopically expressed Gli1 expression vectors in A549 and H23 cells that also stably expressed the siRNA RACK1 6# (Si RACK1 6#). Forced Gli1 expression in a dose-dependent fashion significantly blocked the apoptosis (Fig. 4*A* and supplemental Fig. S3), inhibition of cell migration (Fig. 4*B*), and inhibition of GLIBS luciferase activity, which had been mediated by silencing RACK1 in these NSCLC cell lines with or without Shh-N stimulation (Fig. 4*C*). Also, stably enforced expression of Gli1 in A549 NSCLC cells profoundly reversed the ability of knockdown of RACK1 to inhibit tumor growth in BNX nude mice (Fig. 4*D*). Overall, these data indicate that RACK1 plays a key role in cell survival, migration, and tumor growth, and these oncogenic effects of RACK1 are dependent at least in part on the Shh/GLI1 signaling pathway.

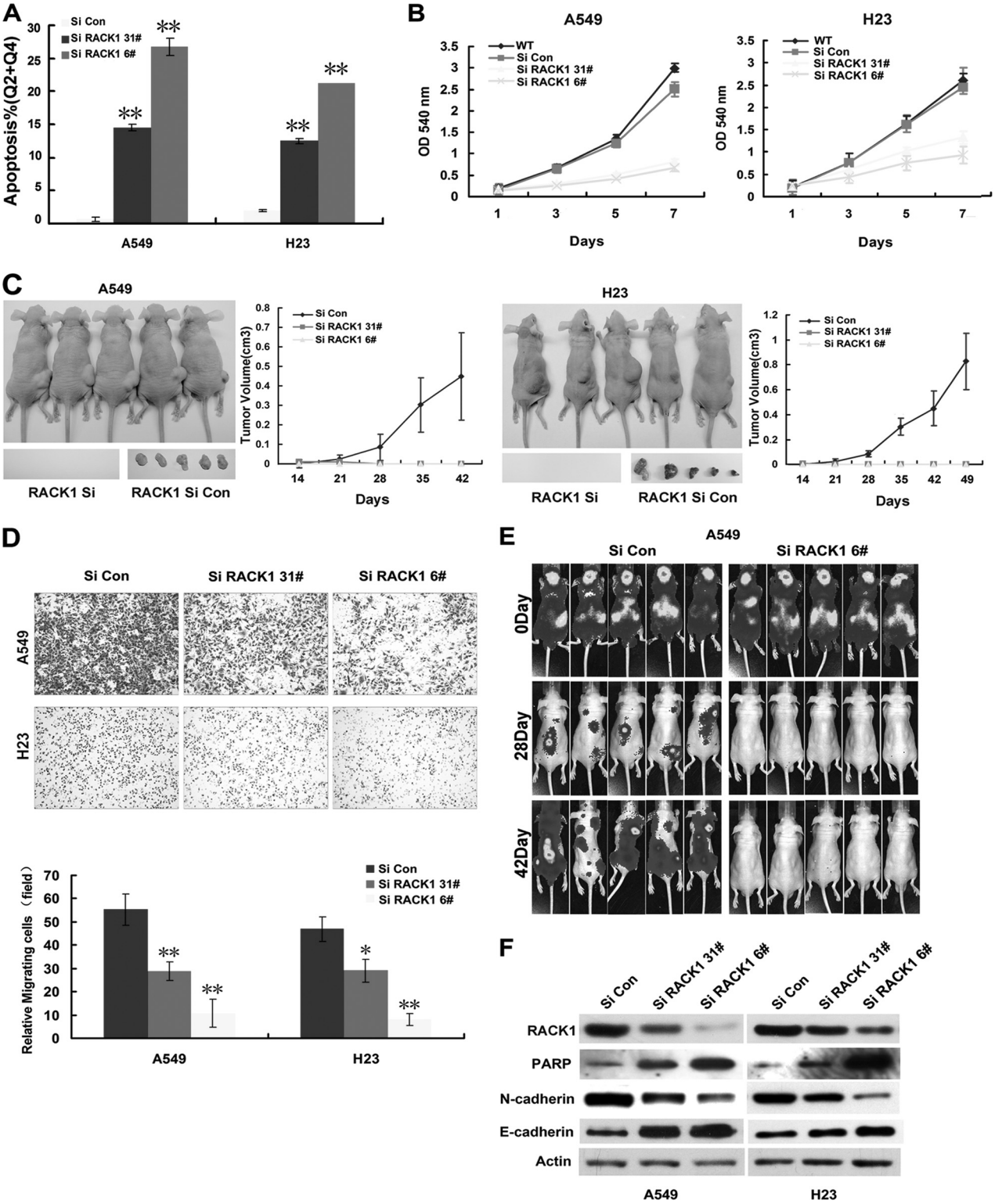

FIGURE 2. **Knockdown of RACK1 promotes cellular apoptosis, inhibits cell growth, and migration.** Both A549 and H23 cell lines were infected with either siRNA RACK1 (*Si RACK1*)- or siRNA control (*Si Con*)-containing virus for 8 h. *A*, quantification of apoptotic cells by annexin V-PE/phosphatidylinositol staining and flow-cytometry analysis is shown. *Bar charts* depict the mean ± S.E. of triplicate measurements of quantification of apoptotic cells by RNAi-mediated knockdown of RACK1 in A549 and H23. Statistical significance was determined with Student's *t* test, $n = 3$. **, $p < 0.01$ *versus* Si Con cells. *B*, MTT assays of A549 and H23 Si RACK1 or Si Con cells are shown. *C*, representative pictures 50 days after injection of BNX nude mice with Si Con or Si RACK1 31# or 6# cells (5×10^6 cells/flank) are shown. The *graphs* show tumor growth. *D*, cell migration assays were performed using Boyden Chambers (1×10^5 cells/well in triplicates). A549 or H23 cells that had passed through the filter after 6 h of culture were fixed and photographed. The *upper six panels* show representative densities of cells that migrated. *Lower bar graphs* depict quantification of migrated cells. Statistical significance was determined with Student's *t* test, $n = 3$, *, $p < 0.05$, **, $p < 0.01$ *versus* Si Con cells. *E*, representative bioluminescent images of the animals in either the control or Si RACK1 groups are shown at 0, 28, and 42 days after injection of NSCLC cells, depicting the extent of tumor burden. *F*, effective knockdown of RACK1 in NSCLC cell lines was confirmed by Western blot, and these cells were examined for markers of apoptosis and migration, cleaved polyadenosine diphosphate-ribose polymerase (*PARP*), E-cadherin, and N-cadherin.

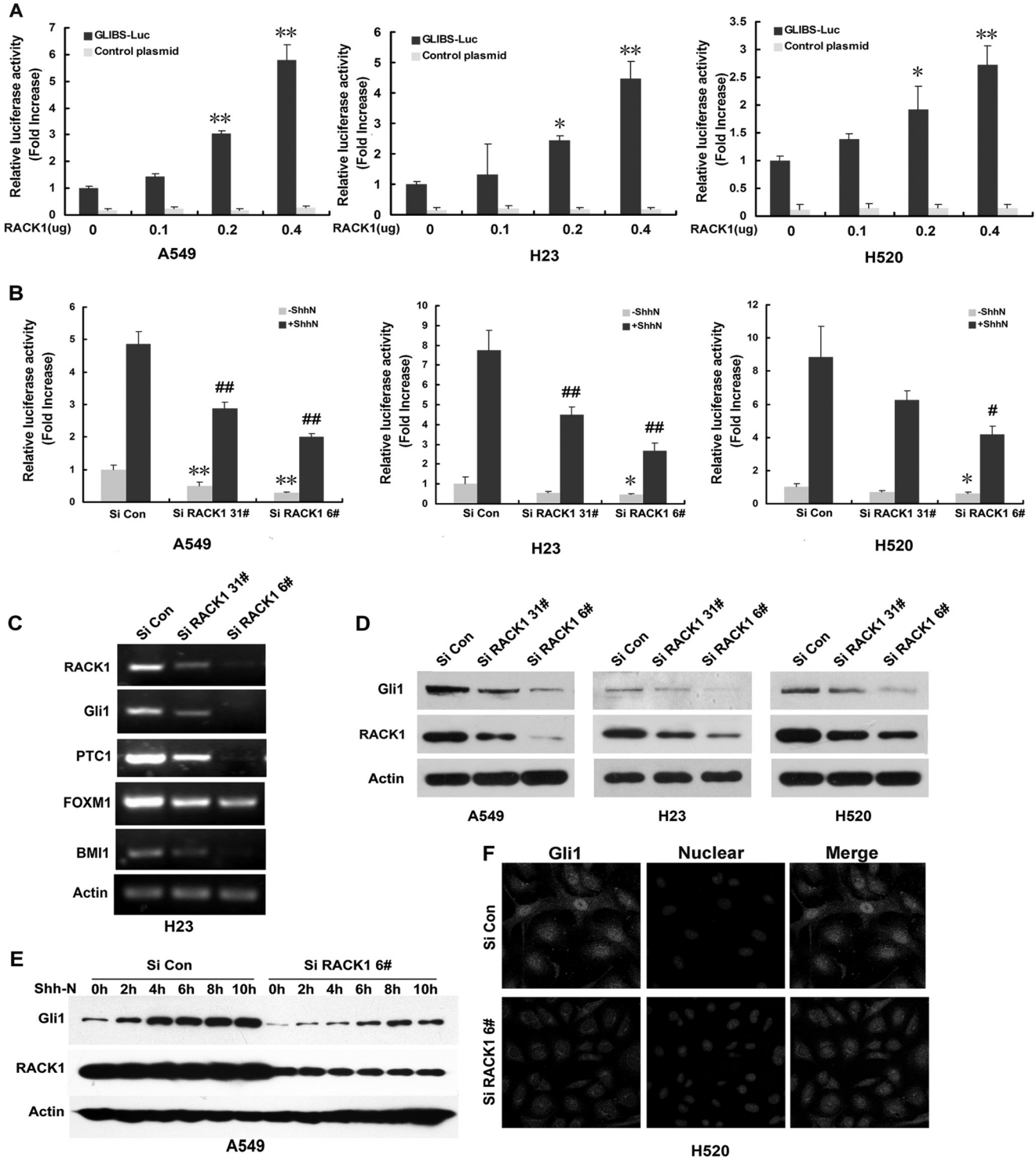

FIGURE 3. **RACK1 up-regulates Gli1 levels and SHH/GLI transcriptional activity.** *A*, SHH/GLI reporter activity was assessed using either multimerized GLI-binding site (*GLI-BS*)-luciferase reporter or TK-luciferase control reporter in NSCLC cells transiently transfected with RACK1 expression vector in a dose-dependent manner (mean ± S.E.; $n = 3$. *, $p < 0.05$; **, $p < 0.01$ *versus* empty vector-transfected cells (RACK1 = 0 μg)). *B*, SHH/GLI reporter activity was assessed using either the multimerized GLI-binding site luciferase reporter or TK-luciferase control reporter in NSCLC cells infected with either Si RACK1 31# or 6# or Si Con-containing virus either with or without Shh-N treatment (mean ± S.E.; $n = 3$. *, $p < 0.05$; **, $p < 0.01$ *versus* Si Con cells without Shh-N (−*Shh-N*); #, $p < 0.05$; ##, $p < 0.01$ *versus* Si Con cells with Shh-N (+*Shh-N*)). *C*, shown is a semiquantitative RT-PCR assay examined level of expression of SHH target gene, Gli1 and Gli1 target gene PTC-1, and FOXM1 and BMI1 expression in the H23 NSCLC cell line. *D*, shown are representative Western blots of three NSCLC cells infected with Si Con and Si RACK1 31#- or 6#-contained virus. β-Actin was used as a loading control. Silencing of RACK1 in NSCLC cells decreased levels of Gli1. *E*, shown is a representative Western blot of A549 cells infected with either Si Con or Si RACK1 6#-containing virus and exposed to Shh-N treatment. Silencing of RACK1 impaired the Gli1 accumulation induced by Shh-N. *F*, shown are photomicrographs of H520 Si Con and Si RACK1 6# cells immunostained with an anti-Gli1 antibody (*red*). Cell nuclei were counterstained with Hoechst (*blue*).

Correlation between RACK1 and Gli1 Expression in NSCLC—Based on our findings that RACK1 was highly expressed in human NSCLC and that RACK1-mediated tumorigenicity in NSCLC was mainly dependent on Shh/GLI signaling pathway, we predicted that RACK1 and Gli1 expression levels would be well correlated in primary NSCLC cancer. The same 63 paired NSCLC samples used to profile RACK1 expression (Fig. 1*A*) were also examined for Gli1 expression levels by real-time PCR. Gli1 mRNA was highly expressed in NSCLC samples compared with the paired normal lung tissues, and univariate analysis

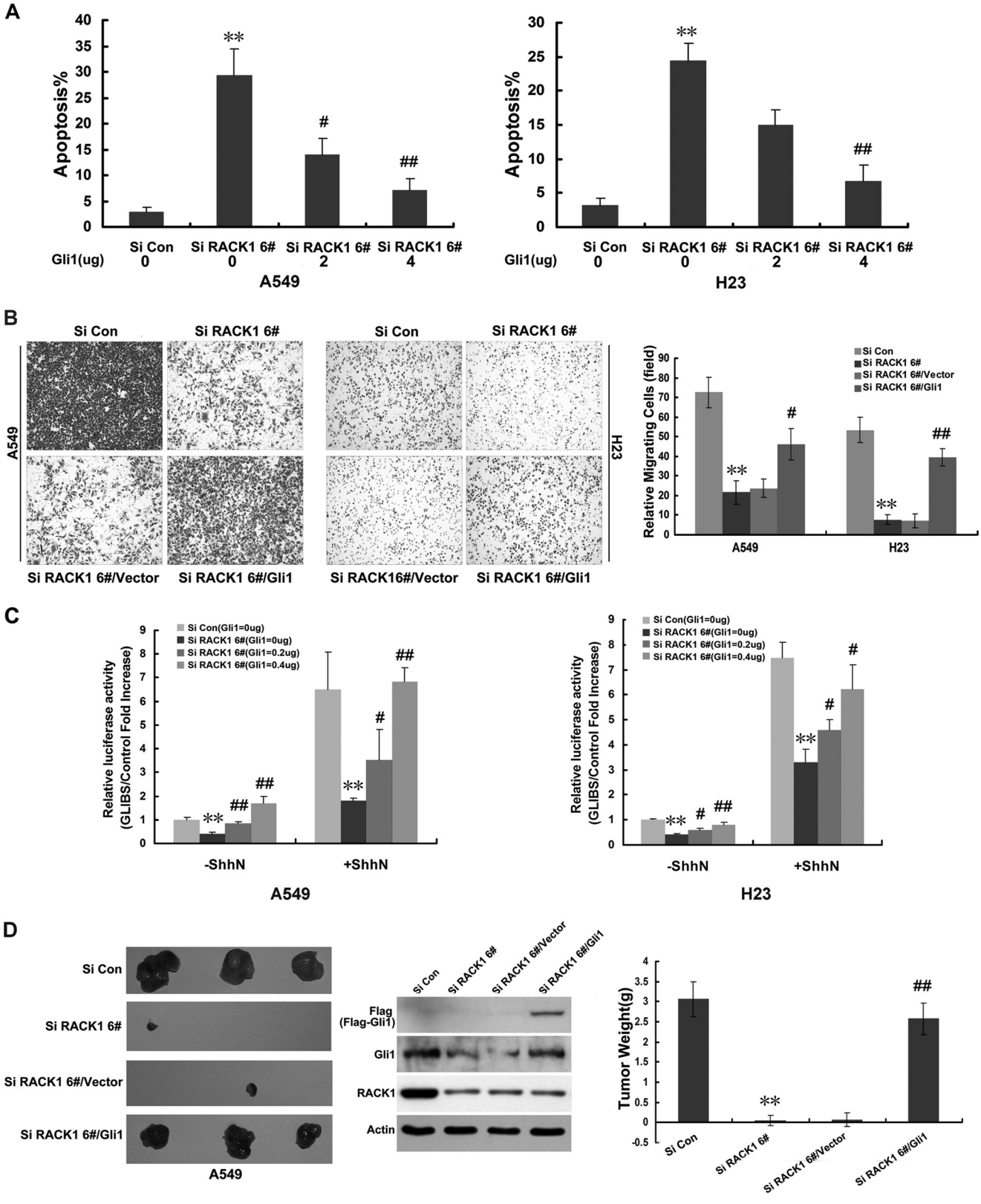

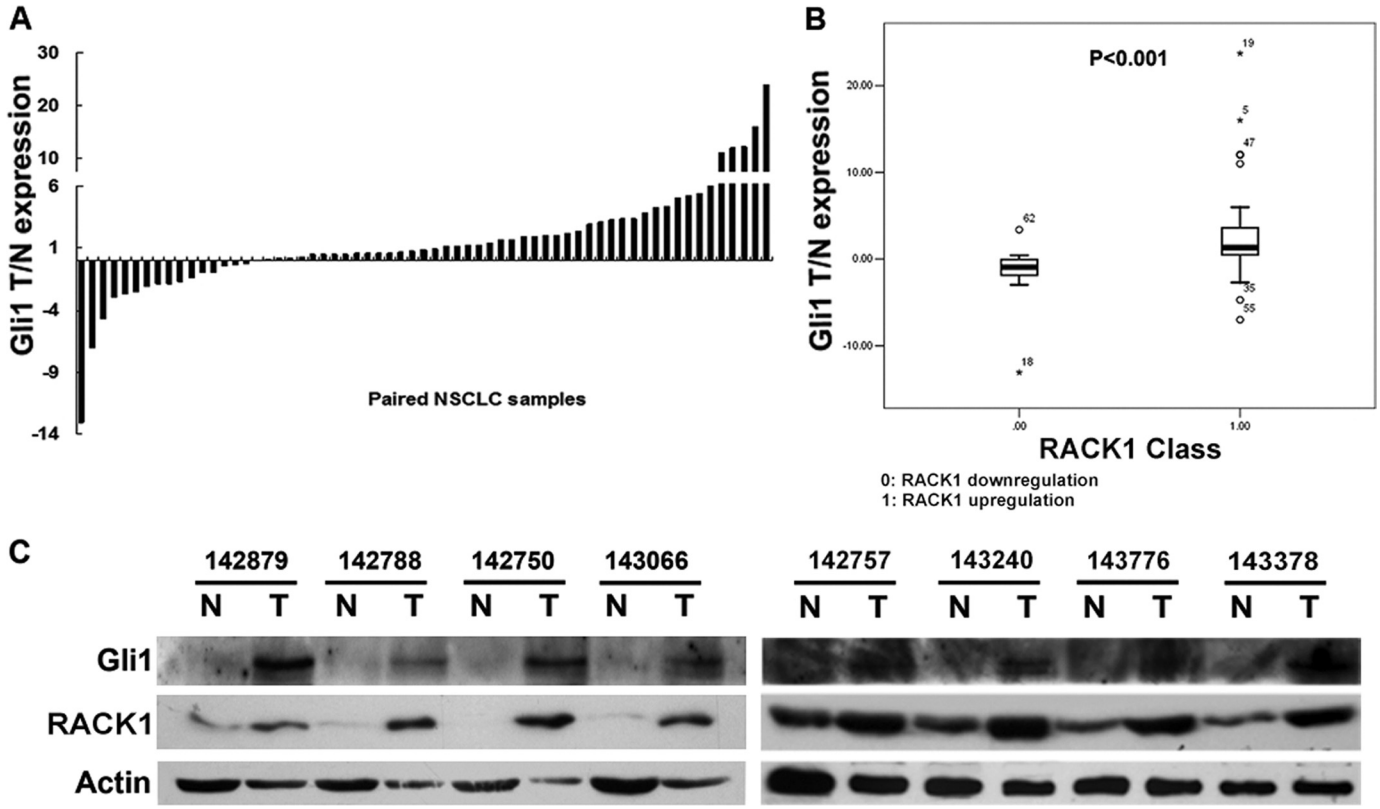

FIGURE 5. **Correlation between Gli1 and RACK1 expression in NSCLC.** *A*, quantitative real time PCR results of relative expression level of Gli1 in 63 pairs of NSCLC and normal lung samples are shown. Gli1 expression levels were normalized to that of β-actin. Data were calculated from triplicates. Each *bar* is the $\log_2$ value of the ratio of Gli1 expression levels between NSCLC (*T*) and matched normal tissues (*N*) from the same patient. Statistical significance was assessed by univariate analysis. *B*, correlation between RACK1 and Gli1 mRNA expression in NSCLC samples is demonstrated by one-way analysis of variance assay. *C*, correlation between RACK1 and Gli1 protein expression in NSCLC samples is demonstrated by Western blot (*T*, NSCLC; *N*, normal lung from same patient).

showed that mRNA levels of Gli1 were significantly different between paired normal and tumor samples ($p = 0.008$) (Fig. 5*A*). Furthermore, a strong negative correlation was found between the level of Gli1 expression and the degree of differentiation of the tumors (supplemental Table 1). Also, the one-way analysis of variance assay showed that RACK1 and Gli1 mRNA expression levels correlated with each other in human NSCLC (Fig. 5*B*). Furthermore, we randomly chose eight pairs of NSCLC samples and found that the protein expression level of Gli1 and RACK1 directly correlated with each other as observed by Western blot (Fig. 5*C*). Taken together, the up-regulation of the SHH signaling pathway by RACK1 may contribute to the development and progression of NSCLC.

RACK1 Interacts and Synergizes with Smo to Activate Gli1 Transcription—The mechanism by which elevated levels of RACK1 increased expression of Gli1 was explored. In the absence of the Hh ligand, PTC inhibits Smo activity. Upon binding of the ligand, PTC no longer inhibits Smo, and Smo is phosphorylated and stabilized (35), and this activated Smo promotes Gli1 transcription and prevents Gli2 and Gli3 cleavage (36). To explore whether RACK1 can increase Gli1 levels by enhancing Smo activity in NSCLC, we treated both Si Con and Si RACK1 6# cells with a Shh-N peptide. The Shh-N stabilized Smo and induced an electrophoretic mobility shift of Smo in Si Con cells. It was well known that an electrophoretic mobility shift of Smo indicates Smo phosphorylation (35, 37–40).

FIGURE 4. **Gli1 was required for the oncogenic effects of RACK1.** *A*, varying amounts of Gli1 expression constructs were transfected into either A549 (*left panel*) or H23 (*right panel*) cells infected with either RACK1 Si Con or RACK1 Si 6# virus. The *bar charts* depict the mean ± S.E. of triplicate measurements of apoptotic cells. **, $p < 0.01$ *versus* Si Con; #, $p < 0.05$; ##, $p < 0.01$ *versus* Si RACK1 6# cells transfected with empty-vector (Si RACK16#, Gli1 = 0). *B*, cell migration assays were performed using Boyden Chamber (1×10^5 cells/well in triplicate). A549 or H23 cells were infected with either Si Con or Si RACK1 6#-containing virus. A549 or H23 Si RACK1 6# cells were stably transfected with either empty vector or Gli1 expression vector (Si RACK1 6#/vector or Si RACK1 6#/Gli1). After 6 h of incubation, cells that passed through the filter were fixed and photographed. The *left panels* show representative densities of cells that migrated. The *right bar chart* depicts the mean ± S.E. of triplicate measurements of migrated cells. **, $p < 0.01$ *versus* Si Con; #, $p < 0.05$ and ##, $p < 0.01$ *versus* Si RACK1 6# cells transfected with empty-vector (Si RACK16#/vector). *C*, varying amounts of Gli1 expression vectors with GLIBS-Luc or TK-luc reporter constructs were cotransfected into two NSCLC cell lines (A549 and H23) that had been infected with either Si Con or Si RACK1 6# expression with or without Shh-N treatment. Forty-eight hours after transfection, GLIBS luciferase reporter assays were performed. Data are presented as the mean ± S.E. $n = 3$. **, $p < 0.01$ *versus* Si Con (Si Con, Gli1 = 0); #, $p < 0.05$ and ##, $p < 0.01$ *versus* Si RACK1 6# cells transfected with empty-vector (Si RACK1 6#, Gli1 = 0). *D*, representative pictures 60 days after injection of two groups of BNX nude mice are shown. One group of mice was injected with either Si Con or Si RACK1 6# cells, and the other group of mice received Si RACK1 6# cells stably transfected with either empty vector or Gli1 expression vector (5×10^6 cells/flank). Tumors were harvested, and protein lysates were Western-blotted and probed for Gli1, FLAG, RACK1, and β-actin. *The bar chart* (*right panel*) shows the mean ± S.E. of triplicate measurements of tumor weight 60 days after injection. **, $p < 0.01$ *versus* Si Con; ##, $p < 0.01$ *versus* Si RACK1 6# cells transfected with empty-vector (Si RACK16#/vector).

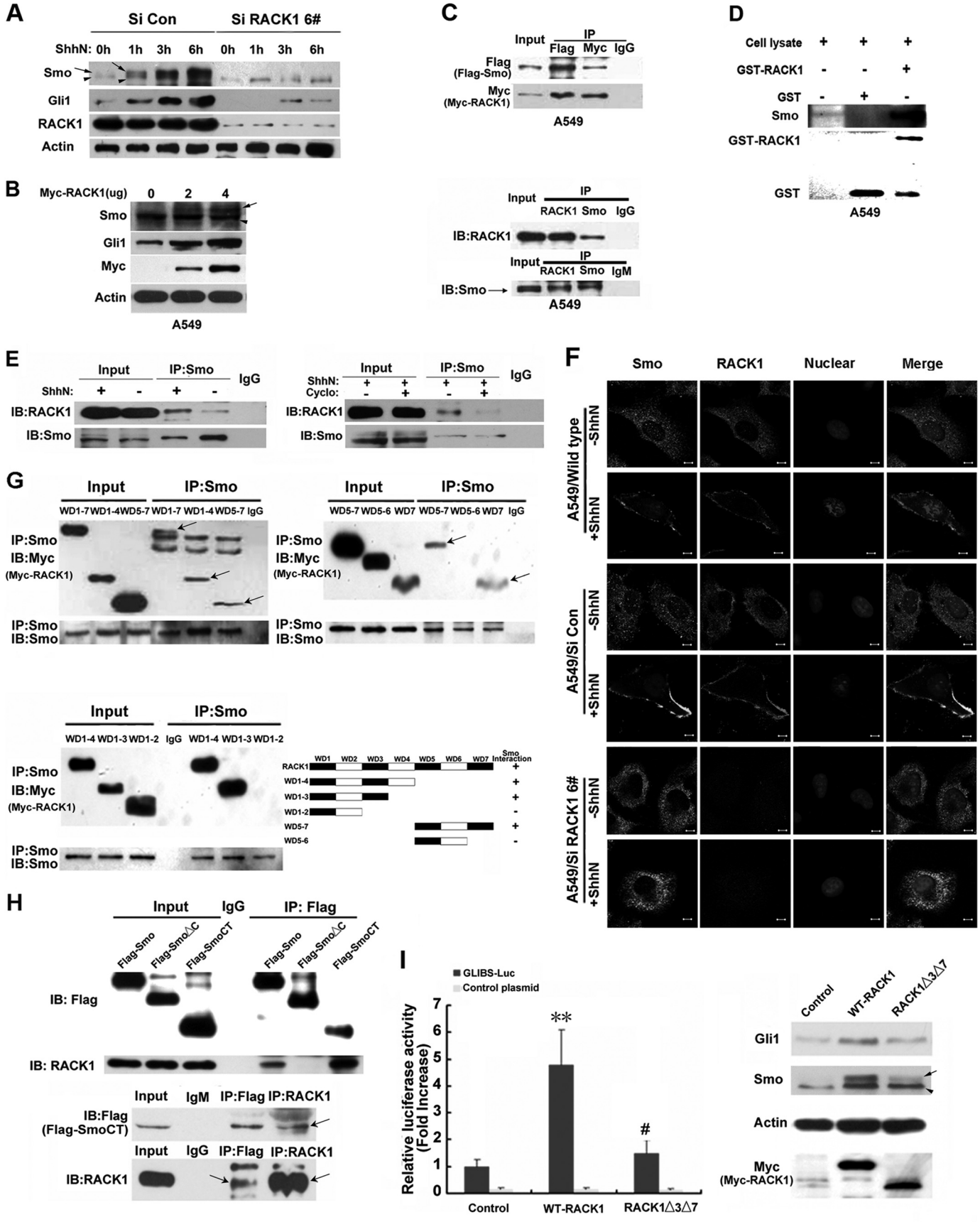
A
Si Con
Si RACK1 6#
ShhN: 0h 1h 3h 6h 0h 1h 3h 6h
Smo
Gli1
RACK1
Actin
B
Myc-RACK1(ug) 0 2 4
Smo
Gli1
Myc
Actin
A549
C
Input
IP
Flag Myc IgG
Flag (Flag-Smo)
Myc (Myc-RACK1)
A549
Input
IP
RACK1 Smo IgG
IB:RACK1
Input
IP
RACK1 Smo IgM
IB:Smo
A549
D
Cell lysate + + +
GST-RACK1 - - +
GST - + -
Smo
GST-RACK1
GST
A549
E
Input
IP:Smo
IgG
ShhN: + - + -
IB:RACK1
IB:Smo
Input
IP:Smo
IgG
ShhN: + + + +
Cyclo: - + - +
IB:RACK1
IB:Smo
F
Smo
RACK1
Nuclear
Merge
A549/Wild type
-ShhN
+ShhN
A549/Si Con
-ShhN
+ShhN
A549/Si RACK1 6#
-ShhN
+ShhN
G
Input
IP:Smo
WD1-7 WD1-4 WD5-7 WD1-7 WD1-4 WD5-7 IgG
IP:Smo
IB:Myc
(Myc-RACK1)
IP:Smo
IB:Smo
Input
IP:Smo
WD5-7 WD5-6 WD7 WD5-7 WD5-6 WD7 IgG
IP:Smo
IB:Myc
(Myc-RACK1)
IP:Smo
IB:Smo
Input
IP:Smo
WD1-4 WD1-3 WD1-2 IgG WD1-4 WD1-3 WD1-2
IP:Smo
IB:Myc
(Myc-RACK1)
IP:Smo
IB:Smo
WD1 WD2 WD3 WD4 WD5 WD6 WD7
Smo Interaction
RACK1 +
WD1-4 +
WD1-3 +
WD1-2 -
WD5-7 +
WD5-6 -
H
Input
IgG
IP: Flag
Flag-Smo
Flag-SmoΔC
Flag-SmoCT
IB: Flag
IB: RACK1
Input
IgM
IP:Flag
IP:RACK1
IB:Flag
(Flag-SmoCT)
Input
IgG
IP:Flag
IP:RACK1
IB:RACK1
I
GLIBS-Luc
Control plasmid
Relative luciferase activity
(Fold Increase)
0 1 2 3 4 5 6 7
**
#
Control
WT-RACK1
RACK1Δ3Δ7
Control
WT-RACK1
RACK1Δ3Δ7
Gli1
Smo
Actin
Myc
(Myc-RACK1)

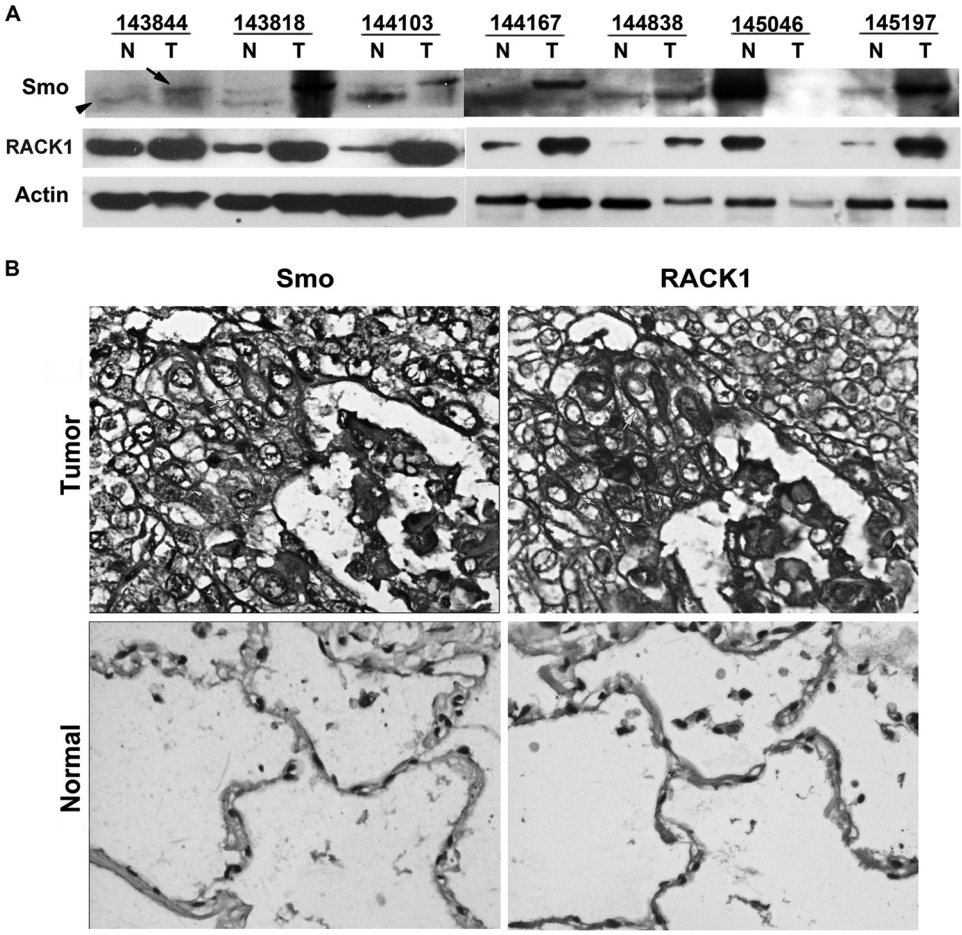

FIGURE 7. **Correlation between RACK1 and Smo expression in NSCLC.** *A*, Western blot analysis of RACK1 and Smo expression in even randomly chosen NSCLC tissues (*T*) and matched normal lung tissues (*N*) (β-actin used as a loading control) is shown. *Arrows* depict the hyperphosphorylated form of Smo, and *arrowheads* depict hypophosphorylated and unphosphorylated forms of Smo. *B*, shown is immunohistochemical staining of human squamous lung carcinoma (sample 145190, *upper panels*) and normal human lung (*lower panels*). Correlation between RACK1 and Smo expression in the squamous lung carcinoma sample is prominent. *Arrows* depict elevated cell membrane and cytoplasmic levels of RACK1 and Smo expression.

Knockdown of RACK1 dramatically diminished the Shh-N induced Smo mobility shift and blocked the accumulation of the hyperphosphorylated form of Smo in Si RACK1 6# cells resulting in less nuclear accumulation of Gli1 (Figs. 6*A* and supplemental Fig. 4*A*). In contrast, overexpression of RACK1 promoted Smo phosphorylation leading to greater accumulation of Gli1 (Fig. 6*B* and supplemental Fig. 4*B*). Furthermore, Shh-N stimulated translocation of RACK1 and Smo from the cycloplasm to the cell membrane causing their colocalization on the cell membrane. In contrast, knockdown RACK1 blocked

FIGURE 6. **RACK1 interacts and activates Smo, leading to Gli1 transcriptional activation.** *A*, electrophoretic mobility shift verifies silencing of RACK1 in A549 cells associated with decrease accumulation of the hyperphosphorylated form of Smo and Gli1 after stimulation by Shh-N. *Arrows* depict the hyperphosphorylated form of Smo, and *arrowheads* depict hypophosphorylated and unphosphorylated forms of Smo. *B*, Western blotting shows overexpression of RACK1 in A549 cells increased the phosphorylation of Smo and the accumulation of Gli1. *Arrows* depict hyperphosphorylated form of Smo, and *arrowheads* depict hypophosphorylated and unphosphorylated forms of Smo. *C*, exogenous and endogenous co-immunoprecipitation assays demonstrate the interaction between Smo and RACK1. Cell lysates of A549 cells were incubated either with anti-RACK1, anti-Smo, anti-FLAG, anti-Myc antibody, or control IgM or IgG. *D*, a GST pulldown assay shows the interaction between Smo and RACK1. Cell lysates of A549 cells were incubated with purified GST or GST-RACK1 protein. The precipitates were detected with anti-GST and anti-Smo antibodies. *E*, an immunoprecipitation assay demonstrates the endogenous interaction between Smo and RACK1 was enhanced in response to Shh-N (*left*) and attenuated by cyclopamine (*Cyclo*) (*right*). A549 cells were untreated or treated with either 50 nM Shh-N or 8 μM cyclopamine as indicated at 37 °C for 4 h. Proteins from cell extracts were immunoprecipitated (*IP*) with an anti-Smo antibody and immunoblotted (*IB*) with an anti-RACK1 antibody. *F*, confocal images of A549 cells immunostained with anti-RACK1 (*red*) and anti-Smo antibodies (*green*) either without or with Shh-N addition (10 min) are shown. Cell nuclei were counterstained with Hoechst (*blue*). RACK1 colocalized with Smo on the cell membrane with Shh-N exposure. Silencing of RACK1 blocked Shh-N stimulated Smo localization onto the cell membrane. *G*, shown is mapping of the interaction between Smo and RACK1. A549 cells were transfected with either wild type Myc-RACK1 construct or different Myc-RACK1 truncated mutants. Cell lysates were immunoprecipitated with an anti-Smo antibody and immunoblotted with an anti-Myc antibody. The third and seventh WD repeats of RACK1 were required for the interaction with Smo. *H*, immunoprecipitation assay verifies that the C-tail of Smo is responsible for the interaction with RACK1. A549 cells were transfected with expression vectors containing either wild type FLAG-Smo, FLAG-SmoCT (Smo C-tail), or FLAG-SmoΔC (Smo lacking its C-tail). Cell lysates were immunoprecipitated with an anti-RACK1 antibody and immunoblotted with an anti-FLAG antibody. The Smo C-tail was responsible for the interaction with RACK1. *I*, GLIBS-luc reporter activity was assessed in A549 cells transfected with either empty vector, wild type Myc-RACK1 vector, or Myc-RACK1Δ3Δ7-truncated mutant (RACK1 lacking its WD3 and -7 domains), showing that Myc-RACK1Δ3Δ7 failed to activate GLI-dependent transcription (*left*) (mean ± S.E.; $n = 3$. **, $p < 0.01$ *versus* empty vector-transfected cells (control); #, $p < 0.05$ *versus* wild-type RACK1 expression vector-transfected cells (WT-RACK1)). Western blotting assays showed that Myc-RACK1Δ3Δ7 lost the ability to elevated Smo phosphorylation and Gli1 accumulation in the absence of Shh-N peptide treatment as compared with wild type Myc-RACK1 (*right*).

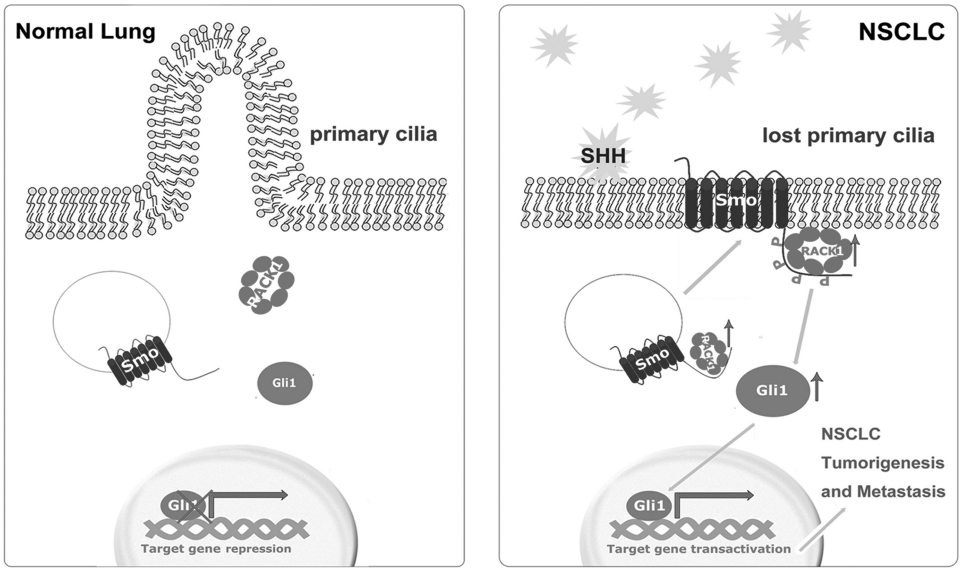

FIGURE 8. **Model of how RACK1 mediates activation of SHH/GLI signaling in NSCLC Cells.** *Left*, normal lung cells have low expression level of RACK1, and Smo is mainly localized in the cytoplasm, not on the cell membrane. Cytoplasmic Smo has little ability to stimulate Gli1 activation. *Right*, NSCLC cells express high levels of RACK1 that binds, transports, and activates Smo on the cell membrane in response to the SHH ligand. This results in translocation of Gli1 from the cytoplasm to the nucleus, leading to increased Gli1 levels and subsequent activation of downstream target genes.

the Shh-N induced Smo accumulation on the cell membrane (Fig. 6*F*). Taken together, these data suggest that RACK1 is required for the activation of Smo, which is induced by Shh ligand.

We further explored how RACK1 regulates Smo activity, which was our next question. Smo is a classical G-coupled receptor (41, 42), and RACK1 is a homologue of the β-subunit of the heterotrimetric G protein. We hypothesized that RACK1 regulates Smo activity by directly interacting with Smo. Both exogenous and endogenous co-immunoprecipitation experiments were performed using A549 and H23 NSCLC cells. The results demonstrated that RACK1 and Smo can interact with each other (Fig. 6*C* and supplemental Fig. 4*C*). To confirm that RACK1 and Smo bind to each other, a GST pulldown assay was performed using purified recombinant RACK1 fused to glutathione *S*-transferase (GST) (GST-RAC-K1) and the lysate from the NSCLC cells. Smo was bound to GST-RACK1 but not to GST (Fig. 6*D*), confirming that RACK1 and Smo bind to each other. In addition, stimulation of Shh-N markedly enhanced RACK1-Smo interaction, whereas cyclopamine, a direct antagonist of Smo, abolished the interaction, suggesting RACK1 interacts with the active form of Smo (Fig. 6*E*).

Recent data suggested that the C-tail of mammalian Smo may be required for activation of Gli1 (35, 43, 44). We found that both FLAG-Smo and FLAG-SmoCT (Smo C-tail), but not FLAG-SmoΔC (Smo lacking its C-tail), co-immunoprecipitated with RACK1 (Fig. 6*H*), demonstrating that the C-tail of Smo is required for the Smo-RACK1 interaction. To narrow the specific binding domain of RACK1 to Smo, a series of truncated mutants of RACK1 was generated. The binding reactions were analyzed by immunoprecipitating with a Smo-specific polyclonal antibody and immunoblotting for RACK1 truncated proteins. Interactions were observed between Smo and the RACK1-truncated mutants having the WD40 repeats 1–4, 5–7, 1–3, and 7 but not these mutants with WD40 repeats 1–2 and 5–6 of RACK1 (Fig. 6*G*), suggesting that at least WD40 3 and 7 domains are necessary for the binding of Smo-RACK1. A truncated form of RACK1 without WD40 3 and 7 (Myc-RACK1Δ3Δ7), in contrast to Myc-RACK1, was no longer able robustly to stimulate GLI-dependent transcription to promote Smo phosphorylation or cause Gli1 accumulation (Fig. 6*I*). In summary, these data demonstrated that RACK1 interacted and activated Smo to enhance nuclear activation of Gli1.

Also, we examined if this close relationship between RACK1 and the active form of Smo occurred in primary NSCLC cancers. Six of seven pairs of randomly chosen NSCLC samples having high RACK1 expression level were noted also to overexpress the active form of Smo (Fig. 7*A*). Also, representative samples of squamous NSCLC (Fig. 7*B*) showed a correlation between RACK1 and Smo expression.

DISCUSSION

Our study has discovered that RACK1 is highly expressed in NSCLC, promoting cell survival and proliferation of NSCLC cells and enhancing their metastatic potential. Furthermore, we have provided evidence that elevated levels of RACK1 correlate with increased Gli1 levels in NSCLC and that silencing of RACK1 decreases activation of both a GLI-mediated reporter as well as target genes of Gli1. In addition, our experiments showed that Gli1 was associated in the oncogenic effects of RACK1 *in vitro* and *in vivo*, and the ability of RACK1 to increase Gli1 levels was attributable to the activation of Smo by RACK1. In summary, our findings implicate RACK1 as an important positive regulator of SHH/GLI-dependent signaling in NSCLC.

RACK1 has been reported to be dysregulated in several cancer types, including oral squamous carcinoma, colon, and breast cancers (45–47). A recent report amplified expression of RACK1 as a biomarker associated with pathological stage, tumor size, and lymph node involvement of pulmonary adenocarcinomas (48), but the mechanisms of how RACK1 levels are

up-regulated in pulmonary adenocarcinomas remain unclear. We observed that the expression of RACK1 was up-regulated in primary, non-small-cell lung cancers, and the levels of this protein correlated with clinic pathological parameters including tumor grade, tumor differentiation, and metastasis status. More importantly, we found that the activation of the Sonic Hedgehog pathway contributed to the tumorigenic role of RACK1 in NSCLC. A large body of data supports the involvement of the hedgehog pathway in NSCLC, but the regulatory mechanism by which hedgehog signaling pathway is activated in NSCLC has been unclear (36). Transcriptional activity of Gli1 is a reflection of the activation of the hedgehog pathway. We found that RACK1 can promote oncogenic transcription and expression of Gli1 in NSCLC cell lines, and the expression pattern of RACK1 parallels the levels of Gli1 in the clinical NSCLC samples. These finding suggest that tumor progression of NSCLC is associated with high levels of RACK1, which stimulates the hedgehog pathway.

When hedgehog binds to PTC, Smo is relieved and activated (49, 50). The activated Smo antagonizes the negative regulators of GLI_A, promoting Gli1 transcription (51). Recent reports showed that in some normal mammalian cells (eg.NIH3T3), Smo requires β-arrestins for activation and translocation to primary cilium to function properly to activate Gli1 (52–54). However, the regulatory mechanism of Smo activation in cancer cells lacking primary cilium (*e.g.* NSCLC) was unexplained. Our study discovered RACK1 was required for the activation of Smo after Shh stimulation in the NSCLC cell lines (supplemental Fig. S5).

The data in the present study support the following model for the mechanism by which RACK1 functions to promote the oncogenesis of NSCLC cells (Fig. 8). In normal lung cells that express low levels of RACK1, activity of Smo is limited by PTCH, resulting in low transcriptional activity of GLI_A. In NSCLC cells, RACK1 is often highly expressed and binds to and activates Smo by phosphorylation after stimulation by the Shh ligand. This results in the translocation of Gli1 from the cycloplasm to the nucleus and subsequent activation of downstream Gli1 target genes. These studies assign an oncogenic role for RACK1 in NSCLC. Besides highlighting RACK1 as a potential biomarker and drug target in NSCLC, the findings define a new mechanism for activating the SHH/GLI signaling pathway in cancer.

Acknowledgments—We thank Dr. David J. Robbins for generously providing GLIBS-Luc reporter constructs TK-luciferase control plasmid and SRαGLI plasmid. We thank Drs. Ariel Ruizi Altaba and Matthew Scott for useful comments regarding Sonic Hedgehog signaling in cancer.

REFERENCES

1. Qiu, Y., Mao, T., Zhang, Y., Shao, M., You, J., Ding, Q., Chen, Y., Wu, D., Xie, D., Lin, X., Gao, X., Kaufman, R. J., Li, W., and Liu, Y. (2010) A crucial role for RACK1 in the regulation of glucose-stimulated IRE1α activation in pancreatic β cells. *Sci. Signal.* **3,** ra7
2. Battaini, F., Pascale, A., Paoletti, R., and Govoni, S. (1997) The role of anchoring protein RACK1 in PKC activation in the ageing rat brain. *Trends Neurosci.* **20,** 410–415
3. Kadrmas, J. L., Smith, M. A., Pronovost, S. M., and Beckerle, M. C. (2007) Characterization of RACK1 function in *Drosophila* development. *Dev. Dyn.* **236,** 2207–2215
4. Mor, I., Sklan, E. H., Podoly, E., Pick, M., Kirschner, M., Yogev, L., Bar-Sheshet Itach, S., Schreiber, L., Geyer, B., Mor, T., Grisaru, D., and Soreq, H. (2008) Acetylcholinesterase-R increases germ cell apoptosis but enhances sperm motility. *J. Cell. Mol. Med.* **12,** 479–495
5. Calura, E., Cagnin, S., Raffaello, A., Laveder, P., Lanfranchi, G., and Romualdi, C. (2008) Meta-analysis of expression signatures of muscle atrophy. Gene interaction networks in early and late stages. *BMC genomics* **9,** 630
6. Hu, L., Lu, F., Wang, Y., Liu, Y., Liu, D., Jiang, Z., Wan, C., Zhu, B., Gan, L., Wang, Y., and Wang, Z. (2006) RACK1, a novel hPER1-interacting protein. *J. Mol. Neurosci.* **29,** 55–63
7. Robles, M. S., Boyault, C., Knutti, D., Padmanabhan, K., and Weitz, C. J. (2010) Identification of RACK1 and protein kinase Cα as integral components of the mammalian circadian clock. *Science* **327,** 463–466
8. Gritli-Linde, A., Bei, M., Maas, R., Zhang, X. M., Linde, A., and McMahon, A. P. (2002) Shh signaling within the dental epithelium is necessary for cell proliferation, growth, and polarization. *Development* **129,** 5323–5337
9. Charytoniuk, D., Porcel, B., Rodríguez Gomez, J., Faure, H., Ruat, M., and Traiffort, E. (2002) Sonic Hedgehog signaling in the developing and adult brain. *J. Physiol. Paris* **96,** 9–16
10. Li, C. L., Toda, K., Saibara, T., Zhang, T., Ono, M., Iwasaki, S., Maeda, T., Okada, T., Hayashi, Y., Enzan, H., Shizuta, Y., and Onishi, S. (2002) Estrogen deficiency results in enhanced expression of Smoothened of the Hedgehog signaling in the thymus and affects thymocyte development. *Int. Immunopharmacol.* **2,** 823–833
11. Bible, K. C., Suman, V. J., Molina, J. R., Smallridge, R. C., Maples, W. J., Menefee, M. E., Rubin, J., Sideras, K., Morris, J. C., 3rd, McIver, B., Burton, J. K., Webster, K. P., Bieber, C., Traynor, A. M., Flynn, P. J., Goh, B. C., Tang, H., Ivy, S. P., and Erlichman, C. (2010) Efficacy of pazopanib in progressive, radioiodine-refractory, metastatic differentiated thyroid cancers. Results of a phase 2 consortium study. *Lancet Oncol.* **11,** 962–972
12. Varjosalo, M., and Taipale, J. (2008) Hedgehog. Functions and mechanisms. *Genes Dev.* **22,** 2454–2472
13. Villavicencio, E. H., Walterhouse, D. O., and Iannaccone, P. M. (2000) The sonic hedgehog-patched-gli pathway in human development and disease. *Am. J. Hum. Genet.* **67,** 1047–1054
14. Toftgård, R. (2000) Hedgehog signaling in cancer. *Cell Mol. Life Sci.* **57,** 1720–1731
15. Gialmanidis, I. P., Bravou, V., Amanetopoulou, S. G., Varakis, J., Kourea, H., and Papadaki, H. (2009) Overexpression of hedgehog pathway molecules and FOXM1 in non-small-cell lung carcinomas. *Lung cancer* **66,** 64–74
16. Yuan, Z., Goetz, J. A., Singh, S., Ogden, S. K., Petty, W. J., Black, C. C., Memoli, V. A., Dmitrovsky, E., and Robbins, D. J. (2007) Frequent requirement of hedgehog signaling in non-small-cell lung carcinoma. *Oncogene* **26,** 1046–1055
17. Scales, S. J., and de Sauvage, F. J. (2009) Mechanisms of Hedgehog pathway activation in cancer and implications for therapy. *Trends Pharmacol. Sci.* **30,** 303–312
18. Borczuk, A. C., Gorenstein, L., Walter, K. L., Assaad, A. A., Wang, L., and Powell, C. A. (2003) Non-small-cell lung cancer molecular signatures recapitulate lung developmental pathways. *Am. J. Pathol.* **163,** 1949–1960
19. Warburton, D., Zhao, J., Berberich, M. A., and Bernfield, M. (1999) Molecular embryology of the lung. Then, now, and in the future. *Am. J. Physiol.* **276,** L697–L704
20. Daniel, V. C., Peacock, C. D., and Watkins, D. N. (2006) Developmental signaling pathways in lung cancer. *Respirology* **11,** 234–240
21. Yagui-Beltrán, A., He, B., Raz, D., Kim, J., and Jablons, D. M. (2006) Novel therapies targeting signaling pathways in lung cancer. *Thorac. Surg. Clin.* **16,** 379–396
22. Lemjabbar-Alaoui, H., Dasari, V., Sidhu, S. S., Mengistab, A., Finkbeiner, W., Gallup, M., and Basbaum, C. (2006) Wnt and Hedgehog are critical mediators of cigarette smoke-induced lung cancer. *PloS One* **1,** e93
23. Warburton, D., and Lee, M. K. (1999) Current concepts on lung development. *Curr. Opin. Pediatr.* **11,** 188–192

24. Velcheti, V., and Govindan, R. (2007) Hedgehog signaling pathway and lung cancer. *J. Thorac. Oncol.* **2,** 7–10
25. Neal, J. W., and Sequist, L. V. (2010) Exciting new targets in lung cancer therapy. ALK, IGF-1R, HDAC, and Hh. *Curr. Treat. Options Oncol.* **11,** 36–44
26. Fujita, E., Khoroku, Y., Urase, K., Tsukahara, T., Momoi, M. Y., Kumagai, H., Takemura, T., Kuroki, T., and Momoi, T. (1997) Involvement of Sonic hedgehog in the cell growth of LK-2 cells, human lung squamous carcinoma cells. *Biochem. Biophys. Res. Commun.* **238,** 658–664
27. Collins, B. J., Kleeberger, W., and Ball, D. W. (2004) Notch in lung development and lung cancer. *Semin. Cancer Biol.* **14,** 357–364
28. Königshoff, M., and Eickelberg, O. (2010) WNT signaling in lung disease. A failure or a regeneration signal? *Am. J. Respir. Cell Mol. Biol.* **42,** 21–31
29. Van Scoyk, M., Randall, J., Sergew, A., Williams, L. M., Tennis, M., and Winn, R. A. (2008) Wnt signaling pathway and lung disease. *Transl. Res.* **151,** 175–180
30. Paul, S., and Dey, A. (2008) Wnt signaling and cancer development. Therapeutic implication. *Neoplasma* **55,** 165–176
31. He, B., Barg, R. N., You, L., Xu, Z., Reguart, N., Mikami, I., Batra, S., Rosell, R., and Jablons, D. M. (2005) Wnt signaling in stem cells and non-small-cell lung cancer. *Clin. Lung Cancer* **7,** 54–60
32. Xie, J., Murone, M., Luoh, S. M., Ryan, A., Gu, Q., Zhang, C., Bonifas, J. M., Lam, C. W., Hynes, M., Goddard, A., Rosenthal, A., Epstein, E. H., Jr., and de Sauvage, F. J. (1998) Activating Smoothened mutations in sporadic basal-cell carcinoma. *Nature* **391,** 90–92
33. Yauch, R. L., Gould, S. E., Scales, S. J., Tang, T., Tian, H., Ahn, C. P., Marshall, D., Fu, L., Januario, T., Kallop, D., Nannini-Pepe, M., Kotkow, K., Marsters, J. C., Rubin, L. L., and de Sauvage, F. J. (2008) A paracrine requirement for hedgehog signaling in cancer. *Nature* **455,** 406–410
34. Rubin, L. L., and de Sauvage, F. J. (2006) Targeting the Hedgehog pathway in cancer. *Nat. Rev. Drug. Discov.* **5,** 1026–1033
35. Zhao, Y., Tong, C., and Jiang, J. (2007) Hedgehog regulates smoothened activity by inducing a conformational switch. *Nature* **450,** 252–258
36. Huangfu, D., and Anderson, K. V. (2006) Signaling from Smo to Ci/Gli. Conservation and divergence of Hedgehog pathways from *Drosophila* to vertebrates. *Development* **133,** 3–14
37. Apionishev, S., Katanayeva, N. M., Marks, S. A., Kalderon, D., and Tomlinson, A. (2005) *Drosophila* Smoothened phosphorylation sites essential for Hedgehog signal transduction. *Nat. Cell Biol.* **7,** 86–92
38. Jia, J., Tong, C., Wang, B., Luo, L., and Jiang, J. (2004) Hedgehog signaling activity of Smoothened requires phosphorylation by protein kinase A and casein kinase I. *Nature* **432,** 1045–1050
39. Zhang, C., Williams, E. H., Guo, Y., Lum, L., and Beachy, P. A. (2004) Extensive phosphorylation of Smoothened in Hedgehog pathway activation. *Proc. Natl. Acad. Sci. U.S.A.* **101,** 17900–17907
40. Chen, Y., Sasai, N., Ma, G., Yue, T., Jia, J., Briscoe, J., and Jiang, J. (2011) Sonic Hedgehog dependent phosphorylation by CK1α and GRK2 is required for ciliary accumulation and activation of smoothened. *PLoS Biol.* **9,** e1001083
41. Nehmé, R., Joubert, O., Bidet, M., Lacombe, B., Polidori, A., Pucci, B., and Mus-Veteau, I. (2010) Stability study of the human G-protein-coupled receptor, Smoothened. *Biochim. Biophys. Acta* **1798,** 1100–1110
42. van den Heuvel, M., and Ingham, P. W. (1996) Smoothened encodes a receptor-like serpentine protein required for hedgehog signaling. *Nature* **382,** 547–551
43. Riobo, N. A., Saucy, B., Dilizio, C., and Manning, D. R. (2006) Activation of heterotrimeric G proteins by Smoothened. *Proc. Natl. Acad. Sci. U. S. A.* **103,** 12607–12612
44. Zhao, Y., Tong, C., and Jiang, J. (2007) Transducing the Hedgehog signal across the plasma membrane. *Fly* **1,** 333–336
45. Subauste, M. C., Ventura-Holman, T., Du, L., Subauste, J. S., Chan, S. L., Yu, V. C., and Maher, J. F. (2009) RACK1 down-regulates levels of the pro-apoptotic protein Fem1b in apoptosis-resistant colon cancer cells. *Cancer Biol. Ther.* **8,** 2297–2305
46. Cao, X. X., Xu, J. D., Xu, J. W., Liu, X. L., Cheng, Y. Y., Wang, W. J., Li, Q. Q., Chen, Q., Xu, Z. D., and Liu, X. P. (2010) RACK1 promotes breast carcinoma proliferation and invasion/metastasis *in vitro* and *in vivo*. *Breast Cancer Res. Treat.* **123,** 375–386
47. Wang, Z., Jiang, L., Huang, C., Li, Z., Chen, L., Gou, L., Chen, P., Tong, A., Tang, M., Gao, F., Shen, J., Zhang, Y., Bai, J., Zhou, M., Miao, D., and Chen, Q. (2008) Comparative proteomics approach to screening of potential diagnostic and therapeutic targets for oral squamous cell carcinoma. *Mol. Cell Proteomics* **7,** 1639–1650
48. Nagashio, R., Sato, Y., Matsumoto, T., Kageyama, T., Satoh, Y., Shinichiro, R., Masuda, N., Goshima, N., Jiang, S. X., and Okayasu, I. (2010) Expression of RACK1 is a novel biomarker in pulmonary adenocarcinomas. *Lung Cancer* **69,** 54–59
49. Murone, M., Rosenthal, A., and de Sauvage, F. J. (1999) Sonic hedgehog signaling by the patched-smoothened receptor complex. *Curr. Biol.* **9,** 76–84
50. Stone, D. M., Hynes, M., Armanini, M., Swanson, T. A., Gu, Q., Johnson, R. L., Scott, M. P., Pennica, D., Goddard, A., Phillips, H., Noll, M., Hooper, J. E., de Sauvage, F., and Rosenthal, A. (1996) The tumor-suppressor gene patched encodes a candidate receptor for Sonic hedgehog. *Nature* **384,** 129–134
51. Walterhouse, D. O., Yoon, J. W., and Iannaccone, P. M. (1999) Developmental pathways. Sonic hedgehog-Patched-GLI. *Environ. Health Perspect.* **107,** 167–171
52. Chen, W., Ren, X. R., Nelson, C. D., Barak, L. S., Chen, J. K., Beachy, P. A., de Sauvage, F., and Lefkowitz, R. J. (2004) Activity-dependent internalization of smoothened mediated by β-arrestin 2 and GRK2. *Science* **306,** 2257–2260
53. Meloni, A. R., Fralish, G. B., Kelly, P., Salahpour, A., Chen, J. K., Wechsler-Reya, R. J., Lefkowitz, R. J., and Caron, M. G. (2006) Smoothened signal transduction is promoted by G protein-coupled receptor kinase 2. *Mol. Cell. Biol.* **26,** 7550–7560
54. Kovacs, J. J., Whalen, E. J., Liu, R., Xiao, K., Kim, J., Chen, M., Wang, J., Chen, W., and Lefkowitz, R. J. (2008) Beta-arrestin-mediated localization of smoothened to the primary cilium. *Science* **320,** 1777–1781